



## OPEN MiR- 150 deletion promotes lung tumor growth by upregulating P-STAT3 and ROS in MDSCs

Anqi Qin<sup>1</sup>, Hao Chen<sup>1</sup>, Fan Xu<sup>1</sup>, Wenting Li<sup>2</sup>, Shuai Guo<sup>1</sup>, Ge Zhang<sup>1</sup>, Aihong Zhang<sup>3</sup>, Aihua Zheng<sup>4</sup>, Feng Tian<sup>2</sup> & Quanhui Zheng<sup>1</sup>✉

Lung cancer is the second most common cancer in the world. Myeloid-derived suppressor cells (MDSCs) are important cell populations in the microenvironment of lung cancer, which affects the development and treatment of lung cancer. A large number of studies have shown that miRNA can regulate MDSCs, promoting tumor development. Here we aim to explore the role of miR- 150 on MDSCs in lung tumors. We established lung tumor models by injecting miR- 150 knock-out (miR- 150 KO) mice with LLC subcutaneously. MiR- 150 deletion promoted tumor growth and increased the ratio of MDSCs in tumors. In addition, knockdown of miR- 150 resulted in high serum levels of IL- 6 and G-CSF and promoted the expression of suppressive-associated molecules in MDSCs. In vitro, inhibition of miR- 150 led to increased expression of ROS, IRE1 $\alpha$  and P-STAT3 in MDSCs. In vivo administration of STAT3 inhibitor significantly inhibited tumor growth in miR- 150 KO mice and reduced ROS level in tumor MDSCs. Our results indicated that miR- 150 deletion promotes lung tumor growth by upregulating P-STAT3 and ROS in MDSCs, suggesting that STAT3 inhibitors are effective in blocking the production of ROS in MDSCs lacking miR- 150.

**Keywords** MDSC, MiR- 150, IRE1 $\alpha$ , STAT3, ROS

MDSCs are immunosuppressive cells that can be divided into two subsets, polymorphonuclear MDSCs (PMN-MDSCs) and monocytic MDSCs (M-MDSCs). Review 1:3<sup>1</sup>. The phenotypic characterisation of MDSCs in mice were defined as CD11b<sup>+</sup>Ly6G<sup>+</sup> and CD11b<sup>+</sup>Ly6 C<sup>+</sup> respectively<sup>2</sup>. Review 1 and 2: Accordingly, the markers of humans have been identified as CD33<sup>+</sup>CD11b<sup>+</sup>CD15<sup>+</sup>CD66b<sup>+</sup> and CD11b<sup>+</sup>CD14<sup>+</sup> HLA-DR<sup>low/neg</sup><sup>3</sup>. MDSCs inhibit T cell activity and form an immunosuppressive state in tumors mainly through Arginase1 (Arg1), inducible nitric oxide synthase (iNOS), and indoleamine2,3-dioxygenase (IDO) Review 1:3<sup>4</sup>. Moreover, MDSCs are usually exposed to oxidative stress, resulting in high levels of intracellular reactive oxygen species (ROS). MDSCs also utilize ROS for inhibitory function Review 1:3<sup>5,6</sup>.

MiRNAs are short single-stranded noncoding RNAs that are approximately 22 nucleotides in length and regulate target gene expression through post-transcriptional regulation Review 1:3<sup>7,8</sup>. A large amount of evidence discovered that miR- 150 had necessary regulatory roles in both normal and malignant hematopoiesis<sup>9</sup>. MiR- 150 is intimately associated with acute myeloid leukemia<sup>10,11</sup>. The expression of miR- 150 in MDSCs was reduced in a mouse model of sepsis, and miR- 150 supplementation was found to reduce the expression of pro-inflammatory cytokines IL- 6 and anti-inflammatory cytokines TGF- $\beta$ , IL- 10 and Arg1 in MDSCs<sup>12</sup>. However, little is known about the effects of miR- 150 on lung tumor development by regulating MDSCs.

Review1 and Review2: Lung cancer is the second most common malignancy in the world. Overall lung cancer is divided into two types, non-small cell lung cancer (NSCLC) and small cell lung cancer (SCLC). NSCLC accounts for the majority<sup>13,14</sup>. MiR- 150 has been shown to effectively inhibit tumor growth when delivered to lung cancer cells through liposomes and nanoparticles<sup>15</sup>. In mice with sepsis, the expansion of MDSCs was accompanied by a reduction of miR- 150<sup>12</sup>. We hypothesized that the loss of miR- 150 in the MDSCs would promote lung tumor growth.

In this study, we detected the effect of miR- 150 on MDSCs in transplanted lung tumor mice models, and explored the regulatory mechanism of miR- 150 in MDSCs.

<sup>1</sup>Hebei Key Laboratory for Chronic Diseases, Tangshan Key Laboratory for Preclinical and Basic Research On Chronic Diseases, School of Basic Medical Sciences, North China University of Science and Technology, Tangshan 063210, People's Republic of China. <sup>2</sup>Department of Laboratory Animal Science, Health Science Center, Peking University, Beijing 100083, People's Republic of China. <sup>3</sup>Department of ICU, The Affiliated Hospital of North China University of Science and Technology, Tangshan 063000, People's Republic of China. <sup>4</sup>Emergency department, Worker's Hospital of Tangshan, Tangshan 063000, People's Republic of China. ✉email: 1078209929@qq.com

## Materials and methods

### Mice and cell lines

Conventional miR-150 knockout mice in C57BL/6 background and WT C57BL/6 mice were purchased from The Jackson Laboratory (Stock No: 007750, Bar Harbor, ME) and were raised in the Medical Laboratory Animal Center of North China University of Science and Technology. After reviewing by the Animal Welfare Ethics Committee of North China University of Science and Technology (2023-SY-059), the experimental procedures on mice were carried out in accordance with the regulations of the Animal Management Committee of North China University of Science and Technology. The mice used in the experiment were 6–10 week old males. Lewis Lung Carcinoma (LLC) Review 2: which was widely used to study the mechanism of lung cancer development was purchased from FuHeng Biology (Shanghai, China). When the cell density reached 90 percent of the T25 cell culture flask, the cells were digested and injected subcutaneously into mice. Reviewer 1:  $1 \times 10^6$  LLC were resuspended in 100  $\mu$ l PBS. Each mouse was subcutaneously injected with 100  $\mu$ l suspended cells.

#### ROS detection.

The cellular ROS level was measured with a dichlorodihydro-fluorescein diacetate (DCFH-DA) fluorescence kit (Beyotime). The experiments were conducted according to the instructions. Overall, DCFH-DA was diluted at a ratio of 1:1000 with serum-free medium RPMI.  $1 \times 10^6$  Review 2: BM-derived MDSCs were incubated with the diluted DCFH-DA probe in a 37 °C incubator for 30 min, then washed with PBS three times, and detected the mean fluorescence intensity by Beckman Coulter MoFlo XDP.

#### BM-derived MDSCs isolation and culture.

The cells were isolated from the bone marrow of naïve C57 mice. These cells were incubated in RPMI 1640 medium containing 10% FBS, 20 ng/ml GM-CSF, 20 ng/ml IL-6 and 50  $\mu$ M 2-ME Review 2: and were induced into MDSCs<sup>16</sup>. Transfection was performed after three days of incubation in a 37 °C incubator supplied with 5% CO<sub>2</sub>.

#### Flow cytometry.

The spleen, bone marrow, tumor and peripheral blood of tumor-bearing mice isolated and prepared into a single-cell suspension incubated with Fc block (clone 2.4G2). Then, the samples were labeled with Percp anti-mouse CD11b, PE anti-mouse ly6G, PE anti-mouse ly6 C, PE anti-mouse ly6G and ly6 C, APC anti-mouse ly6G to identify MDSCs on ice. All mAbs were from BD Biosciences or eBioscience™. After 30 min, stained specimens were washed three times with PBS and fixed with 4% paraformaldehyde. The analysis was performed using a Beckman Coulter MoFlo XDP. Data were processed FlowJo software.

#### MiRNAs transfection.

MiR-150 mimics, mimics NC, and miR-150 inhibitors, inhibitors NC were synthesized by ZHONGSHI TON TRU (Tianjin, China). Briefly, Review 2: 1  $\mu$ l Lipo2000 (M5 Hiper Lipo2000 Transfection Reagent) was diluted with 50  $\mu$ l Ultra-MEM (EallBio Life Sciences) and mixed with miRNAs.  $6 \times 10^5$  BM-derived MDSCs were transfected with a final concentration of 100 nM miRNAs in vitro. After 48 h, the transfected cells were collected for subsequent experiments.

#### RNA extraction and RT-qPCR.

Total RNA was extracted from bone marrow-derived MDSCs transfected with miR-150 mimics, NC mimics or miR-150 inhibitors, NC inhibitors MDSCs Review 2: using Superbrilliant® 6 min High-quality RNA Extraction Kit. The cDNAs were synthesized by MonScript™ RTIII Super Mix with dsDNase (Two-Step) or Superbrilliant® TaqMan miRNA Reverse Transcription Kit. Primer sets for arg1, ido1, csf3, inos were used.  $\beta$ -actin was used as the internal control for the mRNA expression, while RNU6B was utilized as the internal control for the miRNA expression. Relative gene expression was determined by using 2X M5 HiPer SYBR Premix EsTaq (with Tli RNaseH) or Superbrilliant® TaqMan miRNA Real Time PCR Mix on a LightCycler 480 quantitative PCR machine (Eppendorf Mastercycler ep realplex). The primers were from Sangon Biotech (Shanghai, China). The primers used are shown in Table 1.

Genes	Primer (5'-3')
IRE1 $\alpha$	TAAGGACAACCCTACCTACAC
	AATTCACGAGCAATGACG
Nos2	GAGCGAGTTGTGGATTGTC
	GAGGGCTTGGCTGAGTGA
CSF3	AGAGGCGCATGAAGCTAAT
	AAGCAAGTCCAAGGTGGG
IDO1	CAGTCCGTGAGTTTGTCA
	CTTTCTCGGTTGTATCTTTC
Arg1	GCTTGCGAGACGTAGACC
	CATCACCTTGCCAATCCC
$\beta$ -actin	CTGTCCCTGTATGCCTCTG
	ATGTCACGCACGATTTC

**Table 1.** Sequence of primers.

## ELISA assay

Reviewer 1 :2. Serum was collected from miR- 150 KO and C57 mice bearing tumors. IL- 6, G-CSF and TGF- $\beta$  from Reviewer 1 :2. serum and culture supernatants were detected with ELISA kits supplied by Shyanzun (Shanghai, China) according to the manufacturer's instructions.

## Western blot analysis

MDSCs after 48 h-transfection with mimics or inhibitors were collected and mingled with RIPA Buffer supplemented with protease inhibitors and phosphatase inhibitors to lyse the cells on ice for 30 min. After then, The NanoDrop 2000 was used to measure protein concentration. 10% SDS-PAGE gel (One Step SDS-PAGE Gel Fast Preparation Kit) was used to separate different groups of proteins in equal amounts. The loading holes were divided into 15 by the comb. MDSCs transfected with miRNA was divided into four groups and added to the pore successively. BM-derived MDSCs of miR- 150 KO and C57 mice were added to the pore, respectively. Proteins were transferred to PVDF membranes, blocked with TBST with 5% skim milk, and incubated with anti-phosphor-STAT3(Tyr705) (ab76315, Abcam), anti-STAT3(ab68153, Abcam), anti-IRE1 $\alpha$  (A17940, ABclonal) primary antibodies overnight at 4 °C. After incubation with the primary antibody, the PVDF membrane containing the protein was washed three times with TBST and incubated with the anti-rabbit HRP-IgG(ReportBio) secondary antibody for 1 h at room temperature. The results were finally detected on a chemiluminescence imaging instrument(Bio-Rad) using the BeyoECL Plus (Beyotime, Shanghai, China).

STAT3 inhibitor S3I- 201 administration.

On the ninth day after the subcutaneous injection of LLC tumors into mice, 5 mg/kg S3I- 201(cayman) or PBS was injected intraperitoneally and continued for two weeks. The drug was injected every other day<sup>17,18</sup>.

Statistics.

All data analyzed in this experiment were expressed as mean  $\pm$  SD. Prism 8 was used for statistical analysis, two independent samples t-test or one-way ANOVA was used for analysis. The value of 0.05 was considered statistically significant.

## Results

### MiR- 150 deletion promoted lung tumor growth

It has previously been reported that a decrease in miR- 150 expression in MDSCs in sepsis leads to the expansion of MDSCs and an increase in Arg1 production<sup>12</sup>. Hence, we hypothesized that the progression of tumors would be affected in the miR- 150 KO mice. MiR- 150 KO mice (Figure. 1a) and the same age of WT mice were subcutaneously inoculated with LLC. We discovered the tumor growth rate of miR- 150 KO mice was significantly faster than that of WT mice (Figure. 1b). At 21 days, there was a significant change in tumor volume, with the tumor volume from miR- 150 KO mice being larger than that from WT mice(Fig. 1c, d). These results suggested that the disappearance of miR- 150 in mice promoted tumor development.

MiR- 150 deletion resulted in an increase in MDSCs.

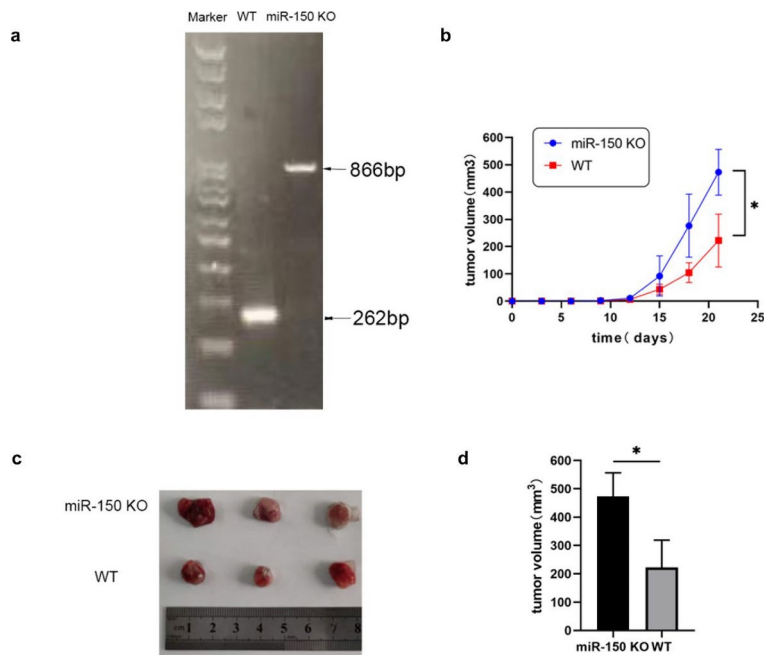


**Fig. 1.** The tumor growth rate of miR- 150 KO mice was significantly accelerated. **(a)** PCR is used to identify the genotype of mice. **(b)** Comparison of tumor growth curves between miR- 150 KO mice and WT mice. **(c-d)** Comparison of tumor size differences at 21 days. \*P < 0.05, \*\*P < 0.01, \*\*\*P < 0.001; ns, no significance.

In addition, We also examined the changes in MDSCs in the tumor. Compared with WT tumor-bearing mice, the M-MDSCs of tumors in miR- 150 KO tumor-bearing mice were obviously increased (Figure. 2a, b). Knockout of miR- 150 also caused amplification of PMN-MDSC in tumors (Figure. 2c, d). M-MDSC had stronger immunosuppressive activity than PMN-MDSC<sup>19</sup>. IL- 6 can increase the mRNA expression of Arg1 in MDSCs<sup>20</sup>. G-CSF can not only regulate the migration of MDSCs but also promote the differentiation and development of BM cells towards MDSCs<sup>21</sup>. The serum of tumor-bearing mice was collected to measure the changes of IL- 6 and G-CSF. In miR- 150 KO tumor-bearing mice, these two cytokines were apparently elevated (Figure. 2e, f). These results revealed that ablation of miR- 150 resulted in an increase in MDSCs, thereby accelerating tumor growth.

MiR- 150 inhibits the expression of factors with suppressive activity in MDSCs.

To determine whether miR- 150 affected the expression of factors with suppressive activity in MDSCs, miR- 150 mimics or inhibitors were transfected into BM-derived MDSCs isolated from WT mice in vitro. After 48

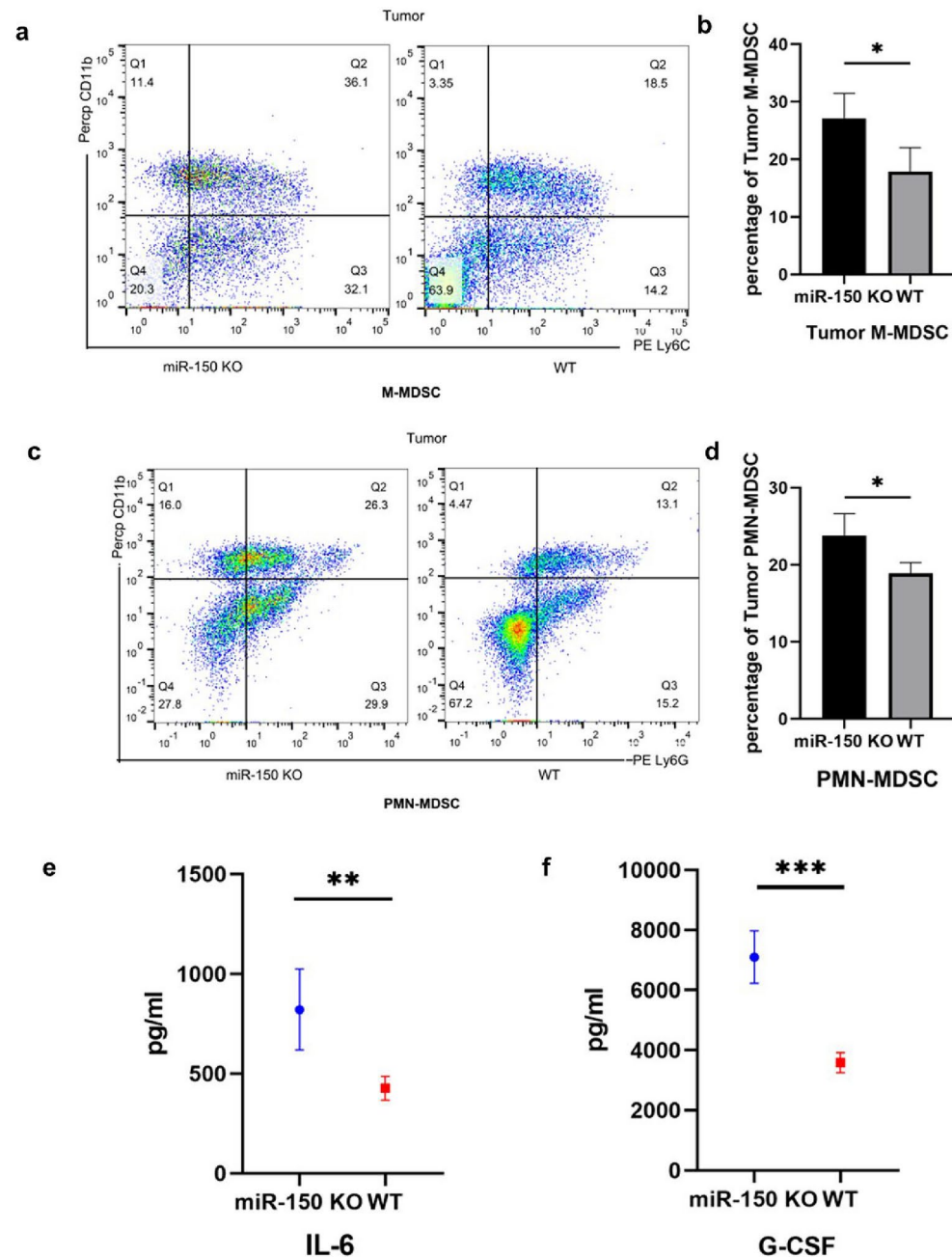


**Fig. 2.** The percentage of MDSCs increased in miR- 150 KO tumor-bearing mice. (a–b) Flow cytometry was used to measure the proportion of M-MDSCs in tumors from miR- 150 KO and WT mice, respectively. Gating CD11b<sup>+</sup> cells for analysis. (c–d) The percentage of PMN-MDSCs in miR- 150 KO and WT tumor-bearing mice. (e–f) ELISA was used to detect changes in serum IL- 6 and G-CSF levels in mice with miR- 150 KO and WT bearing tumors. \*P < 0.05, \*\*P < 0.01, \*\*\*P < 0.001; ns, no significance.

h of transfection, the expression of miR-150 in MDSC was significantly increased or decreased (Fig. 3a). We detected changes in Arg1, G-CSF, iNOS, and IDO1 within its cells. Overexpression of miR-150 significantly reduced the expression levels of inhibitory factors, such as Arg1 (Fig. 3b), iNOS (Fig. 3c), IDO1 (Fig. 3d), and G-CSF (Fig. 3e). Consistent with previous research findings, the increase of miR-150 in MDSC resulted in the loss of its ability to inhibit T cell proliferation and low expression of Arg1<sup>12</sup>. In contrast, the mRNA expression of these inhibitors was significantly elevated after miR-150 was inhibited (Fig. 3 f-i).

MiR-150 suppresses the generation of ROS in MDSC.

The upregulation of ROS in MDSC may inhibit the response of antigen-specific CD8<sup>+</sup> T cells Review 1:3<sup>22</sup>. ROS can also regulate the differentiation of MDSCs, and high levels of ROS can prevent the differentiation of MDSCs into mature cells<sup>23</sup>. High levels of intracellular miR-150 in MDSCs reduced ROS production (Fig. 4a, b), while inhibition of intracellular miR-150 increased ROS production (Fig. 4c, d). We also isolated MDSCs derived from BM of miR-150 KO and WT mice. Consistent with the transfection results, the BM-induced MDSCs in miR-150 KO mice exhibited higher levels of ROS (Fig. 4e, f). These results suggested that miR-150 is involved in the regulation of intracellular ROS production in MDSCs cells.

### MiR-150 decreases the expression of IRE1 $\alpha$ and phosphorylated STAT3 in MDSC

In myeloid cells lacking STAT3, both induced and produced spontaneously ROS were significantly lower than in their wild-type control cells, and STAT3 directly regulates ROS production in myeloid cells<sup>24</sup>. Inositol-requiring enzyme-1A (IRE1 $\alpha$ ) is one of the pathways through which unfolded protein response (UPR) mediates cellular adaptation to endoplasmic reticulum stress. IRE1 $\alpha$  is a dual enzyme with serine/threonine protein kinase and ribonuclease activity<sup>25</sup>. The phosphorylation of STAT3 may occur when UPR is activated<sup>23</sup>. Previous studies have shown that IRE1 $\alpha$  can interact with STAT3 and maintain its activation<sup>26</sup>. IRE1 $\alpha$  has been proven to be a target of miR-150 in human bronchial epithelial cells<sup>27</sup>. Therefore, we aimed to investigate whether miR-150 influenced the changes of IRE1 $\alpha$  in MDSCs, which affected the expression of P-STAT3. P-STAT3 plays an important role in the survival and immunosuppressive function of MDSCs. We tested the expression of IRE1 $\alpha$  in MDSCs transfected with miR-150 mimics or inhibitors. The mRNA expression of IRE1 $\alpha$  decreased after transfection with miR-150 mimics, while increased after transfection with miR-150 inhibitors (Fig. 5a, b). We also measured the protein levels of IRE1 $\alpha$ , which were the same as the mRNA changes (Fig. 5c). The deletion of miR-150 upregulated the expression of IRE1 $\alpha$  (Fig. 5d). The changes of P-STAT3 in MDSC were consistent with IRE1 $\alpha$ . When the expression of miR-150 was upregulated, the phosphorylation level of STAT3 was significantly reduced. However, while miR-150 was downregulated at the intracellular level, the expression of P-STAT3 was elevated (Fig. 5e). Changes have been observed in BM-derived MDSCs from WT and miR-150 KO mice (Fig. 5f). IRE1 $\alpha$  and P-STAT3 from BM-derived MDSC of miR-150 KO mice showed higher expression (Fig. 5g-h). These outcomes implied that miR-150 had an influence on the expression of IRE1 $\alpha$  and P-STAT3 in MDSCs.

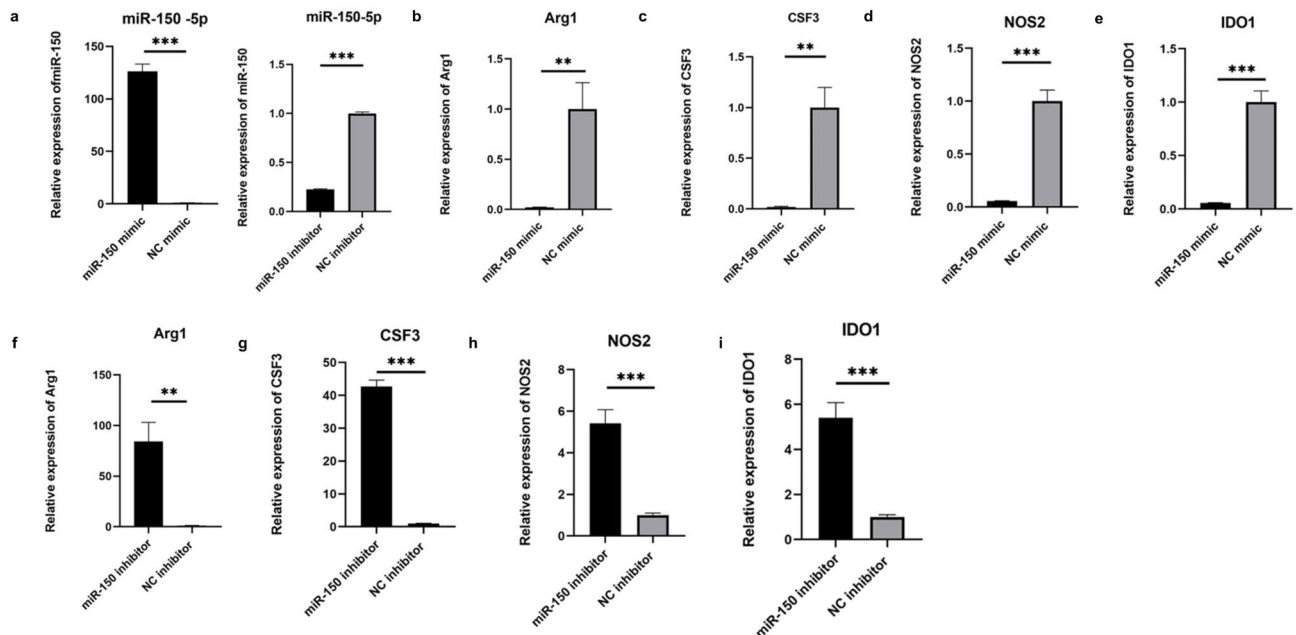


**Fig. 3.** MiR-150 inhibits the expression of prominent factors with suppressive activity in MDSC. (a) qRT-PCR was used to detect the expression of miR-150 in MDSC after transfection. (b-e) Overexpression of miR-150 inhibits the production of immunosuppressive factors in BM-derived MDSCs. (f-i) The inhibition of miR-150 expression conducted more immunosuppressive factors in MDSC. Representative of 3 independent experiments. \*P < 0.05, \*\*P < 0.01, \*\*\*P < 0.001; ns, no significance.

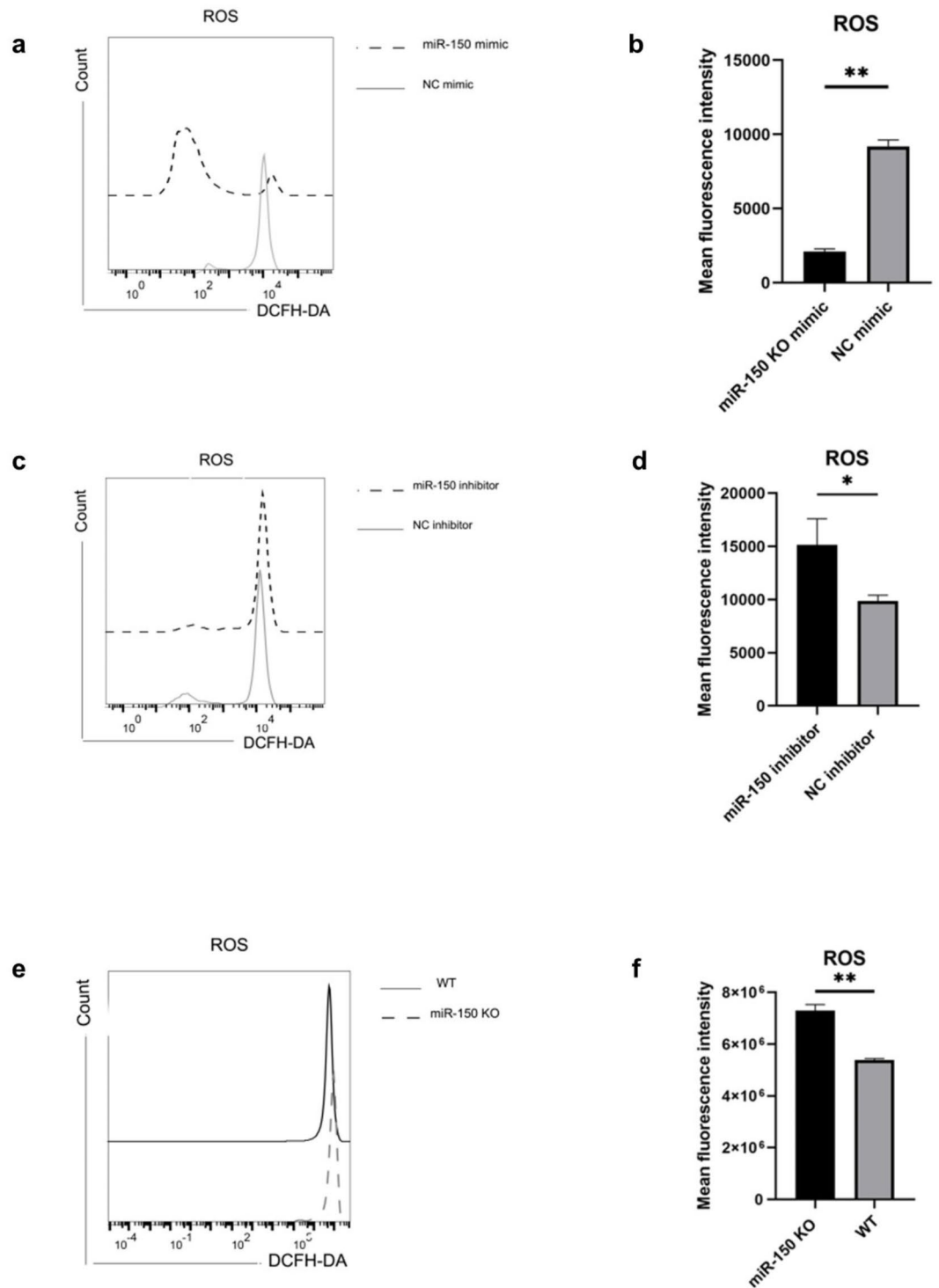


**Fig. 4.** MiR-150 reduces the production of ROS in MDSCs. **(a–b)** The production of ROS was reduced in MDSC transfected with miR-150 mimics. **(c–d)** The downregulation of miR-150 in MDSCs led to an increase in ROS production. **(e–f)** Compared with WT mice, BM-derived MDSCs of miR-150 KO mice showed a significant increase in ROS. \* $P < 0.05$ , \*\* $P < 0.01$ , \*\*\* $P < 0.001$ ; ns, no significance.

#### STAT3 inhibitor S3I-201 suppresses tumor growth by decreasing MDSCs

The above results displayed that P-STAT3 was elevated in MDSCs with low miR-150 expression levels. Previous studies have shown that P-STAT3 exerts an influence on the immunosuppressive function of MDSCs. To determine whether the dysregulation of P-STAT3 caused the advance of tumor growth in miR-150 KO mice, we administered the P-STAT3 inhibitor S3I-201 in vivo. Surprisingly, the speed of tumor growth of miR-150

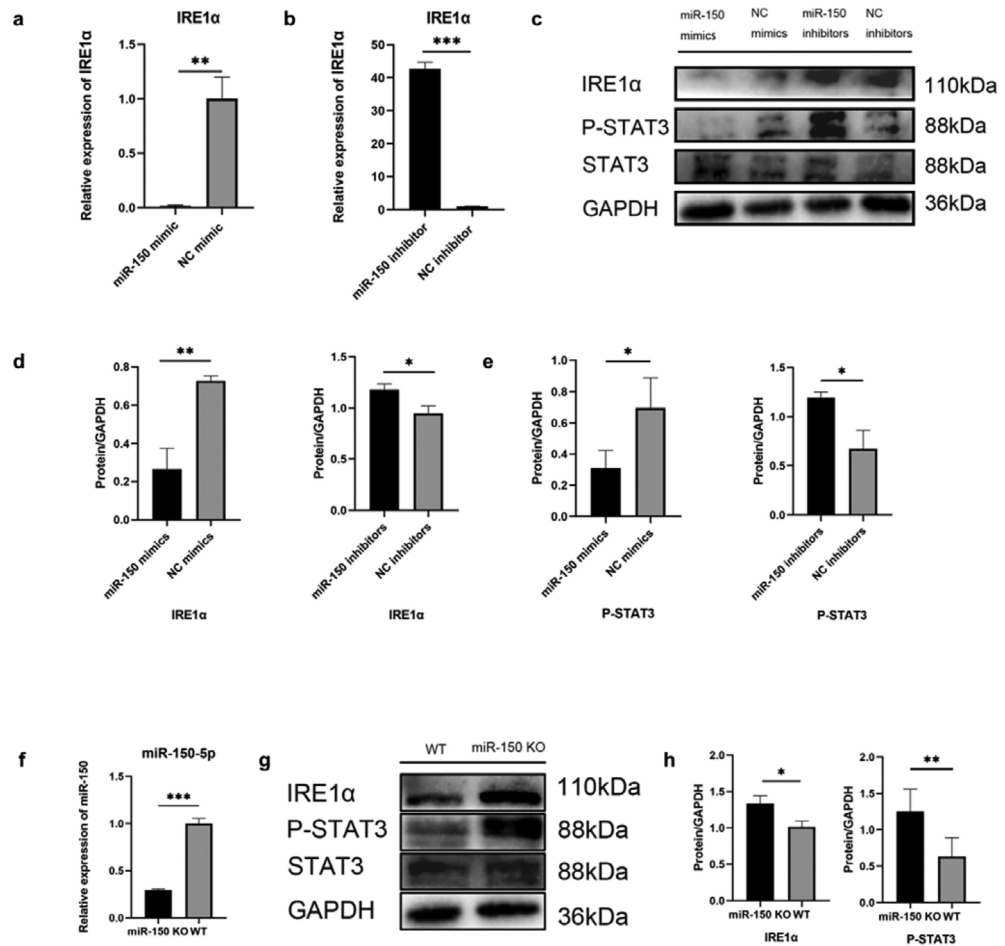


**Fig. 5.** The disappearance of miR-150 augmented the expression of IRE1 $\alpha$  and P-STAT3 proteins in MDSCs. (A–B) qRT-PCR was used to analyze BM-derived MDSC transfected with miR-150 mimics or inhibitors. (C) Western blot was used to detect the expression of IRE1 $\alpha$  and P-STAT3 in BM-derived MDSCs transfected with miR-150 mimics or inhibitors. (D–E) Statistical analysis of IRE1 $\alpha$  or P-STAT3. (F) qRT-PCR validated the lower expression of miR-150 in BM-derived MDSCs of miR-150 KO. (G) Protein analysis of IRE1 $\alpha$  and P-STAT3 in BM-derived MDSC from WT and miR-150 KO mice. (H) Analysis of IRE1 $\alpha$  or P-STAT3 in BM-derived MDSC from WT and miR-150 KO mice. \* $P < 0.05$ , \*\* $P < 0.01$ , \*\*\* $P < 0.001$ ; ns, no significance.

KO mice slowed down (Fig. 6a). The difference in tumor size between miR-150 KO and WT mice was also completely eliminated (Fig. 6b, c).

MDSCs from tumors, peripheral blood, and BM of miR-150-KO, miR-150-KO S3I-201 or WT, and WT S3I-201 mice were harvested for tests. The M-MDSCs of tumors were strikingly reduced in miR-150 KO S3I-201 (Fig. 6d, e), while PMN-MDSC did not diminish in peripheral blood (Fig. 6f, g) and BM (Fig. 6h, i). However, the treatment of S3I-201 failed to reduce the proportion of PMN-MDSC in blood and BM. There was an enhancement in PMN-MDSCs of the blood and BM. However, there was a notable amplification of PMN-MDSCs in the BM of WT S3I-201 mice. This may point out that MDSCs could also expand in a STAT3-independent way. MDSCs were capable of expansion without relying on STAT3<sup>27</sup>. These outcomes suggested that S3I-201 abolished the difference in tumor growth between miR-150 KO mice and WT mice and the proportion of M-MDSCs was declined in tumors.

### The generation of ROS is declined in MDSC from miR-150 KO mice treated with S3I-201

Meanwhile, we also detected the generation of ROS in MDSC. Interestingly, both intracellular ROS in M-MDSC (Fig. 7a, b) and PMN-MDSC (Fig. 7c, d) showed a remarkable reduction in production in miR-150 KO mice treated with S3I-201 compared to their untreated control group. These *in vivo* results were consistent with the previous *in vitro* results (Fig. 4). These results indicated that miR-150 in MDSC had an impact on ROS production by regulating P-STAT3, further affecting its immunosuppressive function.

### Discussion

In this study, we found that the growth rate of LLC was significantly accelerated in miR-150 KO mice. There was a prominent increase in MDSCs at the tumor site, and PMN-MDSCs in the BM and blood were also dramatically

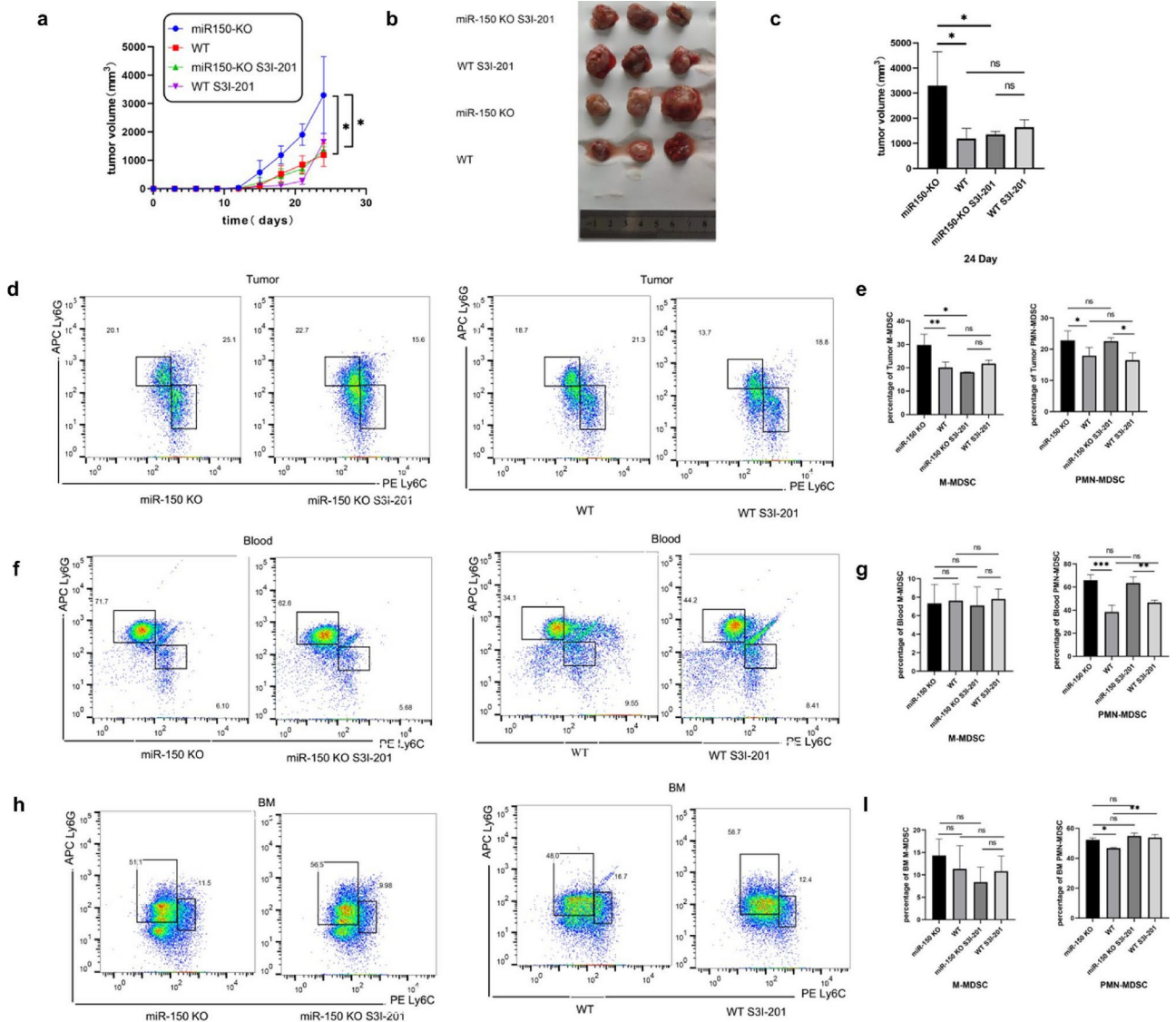


**Fig. 6.** The administration of STAT3 inhibitor S3I- 201 reduced the proportion of M-MDSCs in tumors from miR- 150 KO mice. **(a)** The administration of S3I- 201 delayed the growth of tumors in miR- 150 KO mice. **(b-c)** The treatment of S3I- 201 eliminated the difference in tumor size between miR150-KO and WT mice. **(d-e)** The ratio of MDSC in tumors from miR- 150 KO, WT and their administration groups. **(f-g)** Flow cytometry was used to analysis for MDSCs in peripheral blood from miR- 150 KO, WT and their administration groups. **(h-i)** The changes in the percentage of MDSC in BM of treated or untreated with S3I- 201 groups. MiR- 150 KO S3I- 201 represented the miR- 150 mice treated with S3I- 201 group; WT S3I- 201 represented WT mice treated with S3I- 201 group. \*P < 0.05, \*\*P < 0.01, \*\*\*P < 0.001; ns, no significance.

increased in miR- 150 KO mice. IL- 6 plays a necessary role in increasing the immunosuppressive capacity of MDSC and other myeloid cells<sup>28</sup>. G-CSF can drive bone marrow cells to differentiate into MDSCs, promote MDSC proliferation, and induce MDSC's anti-apoptotic effect<sup>21</sup>. We discovered the levels of IL- 6 and G-CSF were augmented in the serum of miR- 150 KO mice, which coincided with the previous study that reported IL- 6 was downregulated in HK- 2 cells transfected with miR- 150 -5p agomir treatment with LPS<sup>29</sup>. The downregulation of miR- 150 -5p and miR- 543 -3p in MDSC resulted in high levels of G-CSF in the serum of mice<sup>30</sup>. We further detected the expression of G-CSF mRNA in BM-derived MDSCs to determine whether miR- 150 influenced the expression of G-CSF in MDSCs. Our results indicated that miR- 150 could reduce the expression of G-CSF mRNA in MDSCs. Meanwhile, miR- 150 also reduced the expression of other MDSCs-associated suppressive factors, such as Arg1, iNOS, and IDO.

ROS could trigger antigen-specific T cell immune tolerance. The production of ROS is the main mechanism by which bone marrow cells in tumors inhibit T-cell responses<sup>24</sup>. The levels of ROS were strikingly decreased in BM-derived MDSCs transfected with miR- 150, which indicated that miR- 150 could inhibit tumor growth by regulating ROS levels in MDSCs. Therefore, we investigated the regulatory pathways of miR- 150 on ROS production. Many detrimental conditions in the tumor microenvironment(TME) such as hypoxia, nutrient

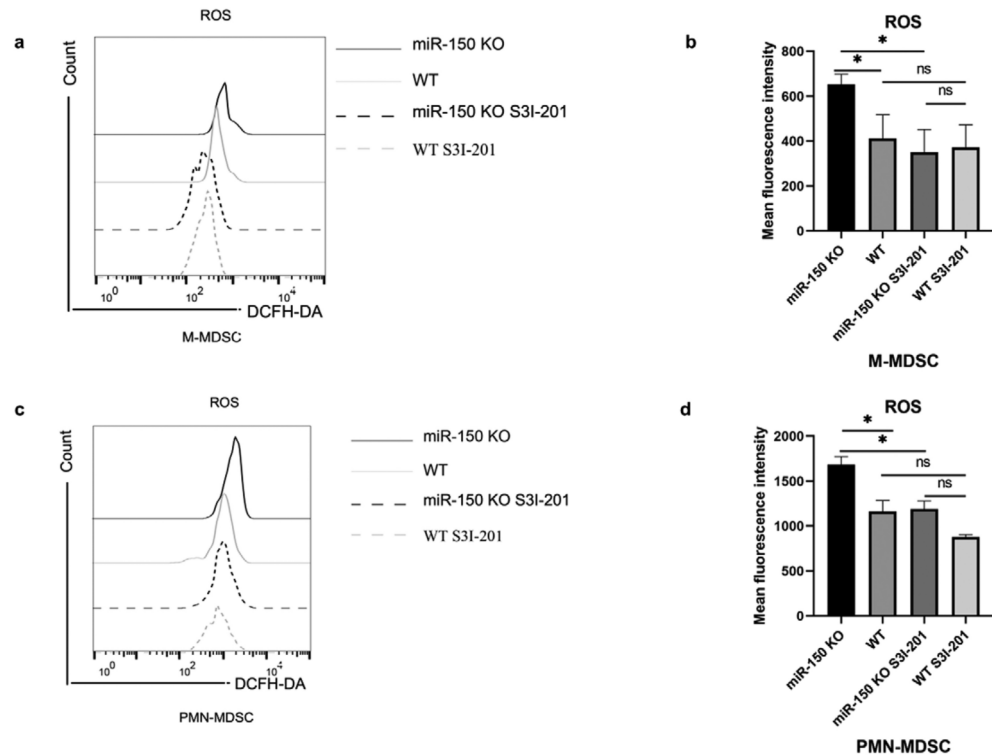


**Fig. 7.** The administration of S3I- 201 downgraded ROS in MDSC from miR- 150 KO mice. (a–b) Detection of ROS in M-MDSC utilizing DCFH-DA probe. (c–d) Flow cytometry was used to detect the average fluorescence intensity of ROS in PMN-MDSC.

deficiency, and increased free radicals in the tumor environment can easily disrupt the protein folding ability of the endoplasmic reticulum (ER), thereby inducing ER stress. MDSCs show objective signs of ER stress response<sup>31</sup>. The accumulation of misfolded proteins triggers the unfolded protein reaction (UPR). IRE1 $\alpha$  is one of the three classic pathways to UPR<sup>25</sup>. STAT3 is involved in the production of ROS in MDSCs<sup>32</sup>. ER stress is closely associated with the STAT3 signaling pathway<sup>33</sup>.

Reports have shown that MDSCs derived from tumor sites have a higher degree of ER stress, expression of IRE1 $\alpha$  and its phosphorylated protein, and ability to inhibit T cell proliferation compared to MDSCs derived from the spleen<sup>34</sup>. ROS scavenging attenuates the total and phosphorylated levels of IRE1 $\alpha$ , resulting in reduced expression of iNOS and Arginase1 in vitro<sup>35</sup>. Deletion of IRE1 $\alpha$  completely abolished the inhibitory activity of PMN-MDSCs in spleen and tumors. Tumor-associated M-MDSCs significantly upregulated Erp72, a protein downstream of IRE1 $\alpha$  and ATF6 pathways<sup>36</sup>. In HBECS, miR- 150 -5p targets IRE1 $\alpha$ , which is one of the ER stress sensor proteins<sup>27</sup>. Overexpression of miR- 150 repressed the expression of IRE1 protein. MiR- 150 targeted the expression of IRE1 $\alpha$  protein in MDSCs. IRE1 $\alpha$ -STAT3 axis assists pro-tumorigenic polarization in macrophages<sup>37</sup>. IRE1 $\alpha$  maintains the activation status of STAT3, and phosphorylation activation of IRE1 $\alpha$  is not a necessary condition for interaction with STAT3<sup>26</sup>. To further explore whether miR- 150 targeting IRE1 $\alpha$  in MDSC influenced the expression of P-STAT3 protein, we detected the P-STAT3 protein in MDSCs. After overexpression of miR- 150, P-STAT3 protein was decreased. MiR- 150 targeting IRE1 $\alpha$  had an impact on the expression of P-STAT3 in MDSCs. Previous studies have found that P-STAT3 can bind to the ARG1 promoter and regulate ARG1<sup>38</sup>. Reviewer 1:3. Recent studies have also shown that STAT3 signaling is essential for MDSC expansion, Arg1 secretion and polyamine production<sup>39</sup>. The elimination of miR- 150 led to an increase in IRE1 $\alpha$  and P-STAT3 levels, which may increase the levels of Arg1, iNOS, and IDO mRNA in MDSCs, as well as an increase in ROS production.

Melanoma patients with high levels of activated STAT3 expression in M-MDSCs exhibit shorter progression free survival. In vitro, another inhibitor of STAT3, Napabucasin, can eliminate the inhibitory ability of human M-MDSCs production<sup>40</sup>. Anal squamous cell carcinoma (ASCC) mice with high STAT3 treated with S3I- 201 had a reduced tumor burden and a reduced population of MDSCs and tumor-associated macrophages (TAMs)<sup>41</sup>. To investigate whether STAT3 plays an important regulatory role in miR- 150 deficient MDSCs, we treated miR- 150 KO and WT mice bearing LLC with S3I- 201, P-STAT3 inhibitor. Administration of S3I- 201 in miR- 150 KO mice significantly reduced M-MDSCs in tumors, and it also slowed down the lung tumor growth of miR- 150 KO mice. The result revealed that STAT3 was important for the suppressive function and expansion of M-MDSC. Nonetheless, there was no decrease in PMN-MDSCs in miR- 150 KO mice. There was a slight amplification of PMN-MDSCs in the BM of WT mice treated with S3I- 201. MDSCs may also have STAT3-independent pathways for expansion. Research has shown that the deletion of STAT3 strengthened Fms-like tyrosine kinase 3 (FLt3L)-mediated MDSCs expansion<sup>42</sup>.

Intriguingly, the generation of ROS in MDSCs was significantly weakened after treatment with S3I-201 in miR-150 KO mice. MiR-150 attenuated the generation of ROS by inhibiting P-STAT3. Further study is needed to explore the distinctions in miR-150 regulation of PMN-MDSC and M-MDSC. More researches are needed to clarify the fine regulation of MDSC by miR-150 in tumors.

In summary, our study suggested that the accelerated lung tumor growth caused by miR-150 deletion was due to an increase in MDSCs. Silencing miR-150 not only led to increased MDSCs in tumors, but also the expression of immunosuppressive molecules such as ROS and Arg1, as well as the levels of IL-6 and G-CSF in serum. The downregulation of miR-150 led to an increase in IRE1 $\alpha$ , which in turn increased the phosphorylation of STAT3. Inhibiting the expression of STAT3 in miR-150 KO mice slowed down lung tumor growth, reduced M-MDSCs in tumors, and ameliorated ROS production in MDSCs. MiR-150 deletion promotes lung tumor growth by upregulating IRE1 $\alpha$ , P-STAT3 and ROS in MDSCs.

## Data availability

All data generated or analysed during this study are included in this published article.

Received: 31 October 2024; Accepted: 5 April 2025

Published online: 15 April 2025

## References

- He, et al. Regulation of T cells by myeloid-derived suppressor cells: emerging immunosuppressor in lung cancer. *Discov. Oncol.* **14**(1), 185 (2023).
- Hegde, S., Leader, A. M. & Merad, M. MDSC: Markers, development, states, and unaddressed complexity. *Immunity* **54**(5), 875–884 (2021).
- Zhang, et al. MDSCs in sepsis-induced immunosuppression and its potential therapeutic targets. *Cytokine Growth Factor Rev.* **69**, 90–103 (2023).
- Goldmann, O., Nwofor, O. V., Chen, Q. & Medina, E. Mechanisms underlying immunosuppression by regulatory cells. *Front. Immunol.* **15**, 1328193 (2024).
- O'Reilly, A., Zhao, W., Wickström, S., Arnér, E. S. & Kiessling, R. Reactive oxygen species: Janus-faced molecules in the era of modern cancer therapy. *J. Immunother. Cancer* **12**(12), e009409 (2024).
- Ohl, K. & Tenbrock, K. Reactive oxygen species as regulators of MDSC-mediated immune suppression. *Front. Immunol.* **9**, 2499 (2018).
- Ameri, et al. Diverse activity of miR-150 in Tumor development: shedding light on the potential mechanisms. *Cancer Cell Int.* **23**(1), 261 (2023).
- Chen, et al. Trends in the development of miRNA bioinformatics tools. *Brief Bioinform.* **20**(5), 1836–1852 (2019).
- He, Y., Jiang, X. & Chen, J. The role of miR-150 in normal and malignant hematopoiesis. *Oncogene* **33**(30), 3887–3893 (2014).
- Huang, et al. MicroRNA-150: A potential regulator in pathogens infection and autoimmune diseases. *Autoimmunity* **48**(8), 503–510 (2015).
- Jiang, X. & Chen, J. miR-150: Targeting MLL leukemia. *Oncotarget* **3**(11), 1268–1269 (2012).
- Liu, et al. MicroRNA-150 inhibits myeloid-derived suppressor cells proliferation and function through negative regulation of ARG-1 in sepsis. *Life Sci.* **278**, 119626 (2021).
- Hendriks, et al. Non-small-cell lung cancer. *Nat. Rev. Dis. Primers.* **10**(1), 71 (2024).
- Li, et al. CircRNA regulates lung cancer metastasis. *Gene* **935**, 149060 (2025).
- Sweef, et al. Unraveling therapeutic opportunities and the diagnostic potential of microRNAs for human lung cancer. *Pharmaceutics.* **15**(8), 2061 (2023).
- Youn, J. I., Nagaraj, S., Collazo, M. & Gabrilovich, D. I. Subsets of myeloid-derived suppressor cells in tumor-bearing mice. *J. Immunol.* **181**(8), 5791–5802 (2008).
- Bu, et al. Targeting STAT3 signaling reduces immunosuppressive myeloid cells in head and neck squamous cell carcinoma. *Oncoimmunology.* **5**(5), e1130206 (2016).
- Wang, Z., Li, J. A., Xiao, W. A., Long, J. & Zhang, H. The STAT3 inhibitor S3I-201 suppresses fibrogenesis and angiogenesis in liver fibrosis. *Lab. Invest.* **98**(12), 1600–1613 (2018).
- Qu, P., Wang, L. Z. & Lin, P. C. Expansion and functions of myeloid-derived suppressor cells in the tumor microenvironment. *Cancer Lett.* **380**(1), 253–256 (2016).
- Weber, et al. IL-6 regulates CCR5 expression and immunosuppressive capacity of MDSC in murine melanoma. *J. Immunother. Cancer.* **8**(2), e000949 (2020).
- Li, et al. G-CSF is a key modulator of MDSC and could be a potential therapeutic target in colitis-associated colorectal cancers. *Protein Cell.* **7**(2), 130–140 (2016).
- Jou, E., Chaudhury, N. & Nasim, F. Novel therapeutic strategies targeting myeloid-derived suppressor cell immunosuppressive mechanisms for cancer treatment. *Explor. Target. Anti-tumor Ther.* **5**(1), 187–207 (2024).
- Romeo, et al. The cross-talk between STAT1/STAT3 and ROS up-regulates PD-L1 and promotes the release of pro-inflammatory/immune suppressive cytokines in primary monocytes infected by HHV-6B. *Virus Res.* **292**, 198231 (2021).
- Corzo, et al. Mechanism regulating reactive oxygen species in tumor-induced myeloid-derived suppressor cells. *J. Immunol.* **182**(9), 5693–5701 (2009).
- Cubillos-Ruiz, J. R., Mohamed, E. & Rodriguez, P. C. Unfolding anti-tumor immunity: ER stress responses sculpt tolerogenic myeloid cells in cancer. *J. Immunother. cancer* **5**, 5 (2017).
- Liu, et al. Role for the endoplasmic reticulum stress sensor IRE1 $\alpha$  in liver regenerative responses. *J. Hepatol.* **62**(3), 590–598 (2015).
- Zhu, M. et al. ROS-responsive miR-150-5p downregulation contributes to cigarette smoke-induced COPD via targeting IRE1 $\alpha$ . *Oxid. Med. Cell. Longev.* **2022**, 5695005 (2022).
- Weber, et al. IL-6 as a major regulator of MDSC activity and possible target for cancer immunotherapy. *Cell Immunol.* **359**, 104254 (2021).
- Shi, et al. MiR-150-5p protects against septic acute kidney injury via repressing the MEK3/JNK pathway. *Cell Signal.* **86**, 110101 (2021).
- Neamah, et al. AhR activation leads to massive mobilization of myeloid-derived suppressor cells with immunosuppressive activity through regulation of CXCR2 and MicroRNA miR-150-5p and miR-543-3p that target anti-inflammatory genes. *J. Immunol.* **203**(7), 1830–1844z (2019).
- Condamine, et al. ER stress regulates myeloid-derived suppressor cell fate through TRAIL-R-mediated apoptosis. *J. Clin. Invest.* **124**(6), 2626–2639 (2014).
- Draghiciu, O., Lubbers, J., Nijman, H. W. & Daemen, T. Myeloid derived suppressor cells—An overview of combat strategies to increase immunotherapy efficacy. *Oncoimmunology* **4**(1), e954829 (2015).

33. Gong, et al. Molecular signal networks and regulating mechanisms of the unfolded protein response. *J. Zhejiang Univ. Sci. B.* **18**(1), 1–14 (2017).
34. Mohamed, et al. The unfolded protein response mediator PERK governs myeloid cell-driven immunosuppression in tumors through inhibition of STING signaling. *Immunity* **52**(4), 668–682.e667 (2020).
35. Mo, et al. ROS Scavenging nanozyme modulates immunosuppression for sensitized cancer immunotherapy. *Adv. Healthc. Mater.* **12**(21), e2300191 (2023).
36. Tcyganov, E. N. et al. Distinct mechanisms govern populations of myeloid-derived suppressor cells in chronic viral infection and cancer. *J. Clin. Invest.* **131**, 16 (2021).
37. Conza, Di. et al. Tumor-induced reshuffling of lipid composition on the endoplasmic reticulum membrane sustains macrophage survival and pro-tumorigenic activity. *Nat. Immunol.* **22**(11), 1403–1415 (2021).
38. Vasquez-Dunddel, et al. STAT3 regulates arginase-1 in myeloid-derived suppressor cells from cancer patients. *J. Clin. Invest.* **123**(4), 1580–1589 (2013).
39. Zhang, et al. VISTA promotes the metabolism and differentiation of myeloid-derived suppressor cells by STAT3 and polyamine-dependent mechanisms. *Cell Rep.* **43**(1), 113661 (2024).
40. Bitsch, et al. STAT3 inhibitor Napabucasin abrogates MDSC immunosuppressive capacity and prolongs survival of melanoma-bearing mice. *J. Immunother. Cancer.* **10**(3), e004384 (2022).
41. Bu, et al. Targeting phosphorylation of STAT3 delays tumor growth in HPV-negative anal squamous cell carcinoma mouse model. *Sci. Rep.* **7**(1), 6629 (2017).
42. Rosborough, et al. Cutting edge: Flt3 ligand mediates STAT3-independent expansion but STAT3-dependent activation of myeloid-derived suppressor cells. *J. Immunol.* **192**(8), 3470–3473 (2014).

## Acknowledgements

This work was supported by grants from the Research Subject of Medical Science from Health Commission of Hebei Province (20190105) and The National Natural Science Foundation of China (81373111). The author would like to thank to all of research participants and the staff at North China University of Science and Technology for their dedication to these studies.

## Author contributions

All authors reviewed the manuscript.

## Declarations

## Competing interests

The authors declare no competing interests.

## Ethics approval

Mice were housed in a specific pathogen-free barrier unit. The animal study protocol was approved by the Animal Care and Use Committee of North China University of Science and Technology, protocol number (2023-SY-059). Experimental procedures adhered to the guidelines set by the committee. All methods were reported in accordance with ARRIVE guidelines. Mice were anesthetized and euthanized by intraperitoneal injection of sodium pentobarbital.

## Additional information

**Supplementary Information** The online version contains supplementary material available at <https://doi.org/10.1038/s41598-025-97556-5>.

**Correspondence** and requests for materials should be addressed to Q.Z.

**Reprints and permissions information** is available at [www.nature.com/reprints](http://www.nature.com/reprints).

**Publisher's note** Springer Nature remains neutral with regard to jurisdictional claims in published maps and institutional affiliations.

**Open Access** This article is licensed under a Creative Commons Attribution-NonCommercial-NoDerivatives 4.0 International License, which permits any non-commercial use, sharing, distribution and reproduction in any medium or format, as long as you give appropriate credit to the original author(s) and the source, provide a link to the Creative Commons licence, and indicate if you modified the licensed material. You do not have permission under this licence to share adapted material derived from this article or parts of it. The images or other third party material in this article are included in the article's Creative Commons licence, unless indicated otherwise in a credit line to the material. If material is not included in the article's Creative Commons licence and your intended use is not permitted by statutory regulation or exceeds the permitted use, you will need to obtain permission directly from the copyright holder. To view a copy of this licence, visit <http://creativecommons.org/licenses/by-nc-nd/4.0/>.

© The Author(s) 2025